

# Phenomenological interpretations of the ac Hall effect in the normal state of $\text{YBa}_2\text{Cu}_3\text{O}_7$

Anatoley T. Zheleznyak<sup>†</sup>, Victor M. Yakovenko<sup>‡</sup>, and H. D. Drew<sup>‡</sup>

Department of Physics and Center for Superconductivity Research, University of Maryland, College Park, Maryland 20742

I. I. Mazin

Computational Science and Informatics, George Mason University and Naval Research Laboratory, 4555 Overlook Ave., Washington DC 20375

(cond-mat/9706029, posted June 3, 1997, revised December 8, 1997)

ac and dc magnetotransport data in the normal state of  $\text{YBa}_2\text{Cu}_3\text{O}_7$  are analyzed within Fermi-liquid and non-Fermi-liquid models. In the Fermi-liquid analysis we use the Fermi surface deduced from band-structure calculations and angular-resolved photoemission experiments and assume that the electron relaxation rate varies over the Fermi surface. The non-Fermi-liquid models are the two-dimensional Luttinger liquid model and the charge-conjugation-symmetry model. We find that the existing experimental data can be adequately fit by any of these models. This work provides a framework for the analysis of experiments that may discriminate among these models.

74.25.Gz, 74.25.Fy, 74.72.-h

## I. INTRODUCTION

The simplest model of the electron transport in metals is the Drude model, where all relaxation processes are described by a single relaxation time  $\tau$  [1]. This model fails to describe the transport properties of high- $T_c$  superconductors in the normal state. Evidence of the failure comes from comparison of the temperature ( $T$ ) dependence of the in-plane resistivity  $\rho_{xx} = 1/\sigma_{xx}$  and the inverse Hall angle  $\cot \theta_H = \rho_{xx}/\rho_{xy}$ , where  $\rho_{xx}$  and  $\rho_{xy}$  are the longitudinal and the Hall components of the conductivity tensor. In the Drude model, both  $\rho_{xx}$  and  $\cot \theta_H$  are proportional to the scattering rate  $1/\tau$ , and therefore should have the same temperature dependence. Experiments, however, show a linear temperature dependence for  $\rho_{xx}$  and  $T^2$  dependence for  $\cot \theta_H$  [2,8]. Additional evidence comes from the frequency ( $\omega$ ) dependence of the Hall coefficient  $R_H = \rho_{xy}/(\omega \rho_{xx} - \omega^2 \rho_{yy})$  and the inverse Hall angle  $\cot \theta_H$  in  $\text{YBa}_2\text{Cu}_3\text{O}_7$  thin films [9]. The experimental data is shown in the upper and lower panels of Fig. 1, where the solid circles represent the real parts ( $\text{Re}$ ) and the solid squares represent the imaginary parts ( $\text{Im}$ ) of  $R_H(\omega)$  and  $\cot \theta_H(\omega)$ . While the inverse Hall angle has a frequency dependence consistent with the Drude model:  $\text{Re} \cot \theta_H(\omega) = \text{const}$  and  $\text{Im} \cot \theta_H(\omega) \propto \omega$  (the lower panel in Fig. 1), the Hall coefficient  $R_H(\omega)$  exhibits non-Drude behavior (the upper panel in Fig. 1). Indeed, in the single-relaxation-time model  $\text{Re} R_H$  is frequency independent, and  $\text{Im} R_H = 0$ ; whereas experimentally  $\text{Re} R_H$  changes by a factor of 3 from  $\omega = 0$  to  $\omega = 200 \text{ cm}^{-1}$ , and  $\text{Im} R_H(\omega) \neq 0$  [10].

In order to explain different temperature dependences of  $\rho_{xx}$  and  $\cot \theta_H$ , Anderson [11] suggested that the transport properties of cuprates are governed by two distinct relaxation times  $\tau_{tr}/T^1$  and  $\tau_H/T^2$ . The first relaxation time controls the longitudinal conductivity, whereas the product of the two times determines the Hall

conductivity:

$$\sigma_{xx} = \frac{\omega_p^2 \tau_{tr}}{4}; \quad \sigma_{xy} = \frac{\omega_p^2 \omega_H \tau_H}{4}. \quad (1)$$

In a conventional model, the coefficients  $\omega_p$  and  $\omega_H$  in Eq. (1) would be the plasma and the cyclotron frequencies, but here they are proposed to be related to the dynamical response of the quasiparticles of the two-dimensional (2D) Luttinger liquid. Generalizing Eq. (1) to a finite frequency in a conventional manner:

$$\sigma_j^{-1} = \sigma_j^{-1} - i\omega; \quad j = tr, H; \quad (2)$$

Kaplan et al. [9] produced a good quantitative fit of their magneto-optical data [12]. However, a microscopic justification of Anderson's hypothesis is problematic. Anderson argued that the two relaxation times originate from two different quasiparticles, holons and spinons, in the Luttinger-liquid picture of two-dimensional electron gas [11]. However, distinct kinetic equations for spinons and holons producing two different relaxation times have not been demonstrated explicitly. In a heuristic discussion, the two times were introduced as different coefficients in front of the electric and the Lorentz forces in the stationary Boltzmann equation for the electrons [13]. However, this procedure violates Lorentz invariance between the electric and Lorentz forces and contradicts the electron equation of motion, which uniquely determines the force term in the Boltzmann equation. It is problematic to write the kinetic equation of Ref. [13] as a time-dependent Boltzmann equation, because it is not clear whether  $\tau_{tr}$  or  $\tau_H$  should be placed in front of the time derivative of the electron distribution function [14]. Lee and Lee [15] studied the Hall effect in a holon-spinon liquid and found a frequency-independent  $R_H(\omega)$ , the same result as in Refs. [12] and [14], which does not agree with experiment [9]. Abrahams [16] demonstrated that Eq. (1)

can be derived from the Boltzmann equation for the electrons if the scattering integral has two different relaxation times for the electron velocities parallel and perpendicular to the applied electric field. However, this assumption cannot be valid in linear-response theory, where the scattering integral does not depend explicitly on the infinitesimal external electric field. Moreover, Kotliar, Sengupta, and Varma [17] proved in general that it is not possible to obtain the multiplicative rule (1) from a Boltzmann equation for the electrons. They observed that skew scattering, if diverging as  $1/T$ , would produce the temperature dependence of the dc magnetotransport. However, their model predicts that  $R_H(\omega)$  does not depend on  $\omega$ , contradicting the ac experiment [9]. Coleman, Schofield, and Tsvelik [18] proposed that the true quasiparticles may have even and odd charge-conjugation symmetry, and their relaxation is characterized by two different rates  $\tau_f$  and  $\tau_s$ . That assumption requires a Bogolyubov transformation of electrons into Majorana fermions, which implies some sort of Cooper pairing with the total momentum of twice the Fermi momentum. Physical justification for the charge-conjugation symmetry is not clear. Lange [19] demonstrated that the frequency dependence of the Hall constant  $R_H(\omega)$  corresponding to the ansatz (1) and (2) can be naturally obtained within the thermodynamic formalism. However, a microscopic calculation within this formalism is not available yet.

An alternative phenomenological explanation for the temperature dependences of  $\sigma_{xx}$  and  $R_H$  within standard Fermi-liquid theory with the electron scattering rate varying over the Fermi surface was proposed in Refs. [4,5]. A conceptually similar approach [20] was quantitatively successful in describing the Hall coefficient of simple cubic metals. In the approach of Refs. [4,5], the Fermi surface of  $\text{YBa}_2\text{Cu}_3\text{O}_{7-x}$  is assumed to have a specific geometry: large flat regions and sharp corners. The electron scattering rate is assumed to have linear temperature dependence on the flat parts of the Fermi surface and quadratic in the corners. With the appropriate choice of parameters, the longitudinal conductivity is dominated by the contribution from the flat regions, whereas the sharply curved corners control the Hall conductivity, and the model approximately yields the required temperature dependences,  $\sigma_{xx} \propto 1/T$  and  $\sigma_{xy} \propto 1/T^3$  [4,5]. A number of papers examined this approach microscopically: the linear temperature dependence of  $1/\omega$  within the nested-Fermi-liquid model [21] and the distribution of  $1/\omega$  over the Fermi surface within the model of antiferromagnetic fluctuations [22-26]. The degree of quantitative agreement between the experiment and the model by Stojkovic and Pines was debated in Refs. [27]. Using a very different microscopic approach, the formalism of slave bosons, Sadeh, Wang, and Doniach [28] studied the distribution of  $\omega$  over an effective Fermi surface of the t-J model and calculated  $R_H$  using an equation equivalent to our Eqs. (3) and (4). An indirect experimental evidence for the anisotropy of  $\omega$  was found in the angular dependence of magnetoresistance in  $\text{Tl}_2\text{Ba}_2\text{CuO}_6$  [29]. A strong vari-

ation of  $\omega$  over the Fermi surface and the so-called "hot spots" occur not only in the theoretical models of magnetotransport in high- $T_c$  superconductors, but also in organic quasi-one-dimensional conductors [30].

Recent measurements of thermopower [31] produced an evidence that the two lifetimes exist in the cuprate metals even without magnetic field. That would eliminate the theoretical models where the second lifetime has a purely magnetic origin, such as the gauge model [15] and the skew scattering model [17]. The thermopower experiment poses a challenge for Anderson's model [11], where the two lifetimes are associated with the processes normal and tangential to the Fermi surface, because thermopower involves only the normal processes. On the other hand, the charge-conjugation and the Fermi-liquid models, where the two lifetimes exist irrespective of magnetic field, are compatible with the experiment.

In this paper, we generalize the phenomenological Fermi-liquid approach of Refs. [4,5] to finite frequencies. We extract  $R_H(\omega)$  and  $\sigma_{xy}(\omega)$  from Ref. [9] using a model in which different parts of the Fermi surface are characterized by two distinct relaxation times  $\tau_1$  and  $\tau_2$ . Since the two parts of the Fermi surface contribute additively to the conductivity tensor, we call this model the additive two-model. The additive law (6) and (7) of this model is in the contrast to the multiplicative law (1) of Anderson's model. The additive law follows naturally from the Boltzmann equation for the electrons, whereas the multiplicative law has not been derived microscopically.

In our model, we assume that the relaxation times  $\tau_1$  and  $\tau_2$  themselves do not depend on frequency. This assumption does not contradict the experimental fact that  $1/\omega \propto \omega^{-1}$  at high frequencies [32,33], because we restrict our tests to the relatively low-frequency range  $\omega < 200 \text{ cm}^{-1}$ , where the frequency dependence of  $\omega$  is not yet significant.

## II. FITTING $\sigma_{xx}(\omega)$ AND $\sigma_{xy}(\omega)$ IN AN ADDITIVE TWO-MODEL

We consider a layered electronic system consisting of two-dimensional (2D) square lattices parallel to the  $(x,y)$  plane and spaced along the  $z$  axis with the distance  $d$ . A weak magnetic field  $H$  is applied perpendicular to the planes. We neglect coupling between the layers and assume that electrons form a 2D Fermi surface. Different points on the Fermi surface can be labeled by  $k_t$ , the transverse component of the electron wave vector. In general, the electron relaxation time  $\tau(k_t)$  and the Fermi velocity  $v(k_t) = \sqrt{v_x^2(k_t) + v_y^2(k_t)}$  may vary along the Fermi surface. Within the conventional relaxation-time approximation for the Boltzmann equation [1], the components of the frequency-dependent conductivity tensor are given by the following equations:

$$\begin{aligned} \sigma_{xx}(\omega) &= \frac{e^2}{2\pi^2 \hbar d} \int \frac{v_x^2(k_t) \sim (k_t; \omega)}{v(k_t)} dk_t \\ &= \frac{e^2}{(2\pi)^2 \hbar d} \int v(k_t) \sim (k_t; \omega) dk_t; \end{aligned} \quad (3)$$

$$\begin{aligned} \sigma_{xy}(\omega) &= \frac{e^3 H}{(2\pi)^2 \hbar c d} \int dk_t \\ &= \frac{e_z}{v(k_t) \sim (k_t; \omega)} \frac{d[v(k_t) \sim (k_t; \omega)]}{dk_t}; \end{aligned} \quad (4)$$

$$\frac{1}{\omega \sim (k_t; \omega)} = \frac{1}{(k_t)} \quad \omega!; \quad (5)$$

where  $\hbar$  is the Planck constant,  $c$  is the speed of light,  $e$  is the electron charge,  $e_z$  is a unit vector along the  $z$  axis, and the integrals are taken over the Fermi surface. Equation (4) is a finite-frequency generalization of Ong's formula [34], which expresses the Hall conductivity of a 2D system in terms of the area enclosed by the mean-free-path curve. Equation (4) applies when magnetic field is weak:  $\omega_c \ll 1$ , where  $\omega_c = (2eH/\hbar c)[dk_t=v(k_t)]^{-1}$  is the cyclotron frequency corresponding to the electron motion around the Fermi surface [1].

Although in general the scattering rate should be continuously distributed over the Fermi surface, to simplify analysis we consider a model in which the Fermi surface is divided into two regions characterized by different relaxation times  $\tau_1$  and  $\tau_2$ . With this assumption, Eqs. (3) and (4) can be parametrized as follows:

$$\sigma_{xx}(\omega) = \frac{1}{4} [a_1 \tau_1(\omega) + a_2 \tau_2(\omega)]; \quad a_1 + a_2 = 1; \quad (6)$$

$$\sigma_{xy}(\omega) = \frac{1}{4} [b_1 \tau_1^2(\omega) + b_2 \tau_2^2(\omega)]; \quad b_1 + b_2 = 1; \quad (7)$$

$$\frac{1}{\tau_{1,2}(\omega)} = \frac{1}{\tau_{1,2}} \quad \omega!; \quad (8)$$

where

$$\omega_p^2 = \frac{e^2}{\hbar d} \int v(k_t) dk_t; \quad (9)$$

$$\omega_H = \frac{eH}{\hbar c} \int e_z \cdot v(k_t) \frac{dv(k_t)}{v(k_t)} dk_t; \quad (10)$$

$$a_1 = \frac{\int v(k_t) dk_t}{\int v(k_t) dk_t}; \quad (11)$$

$$\frac{b_1}{Z} = \frac{\int e_z \cdot v(k_t) \frac{dv(k_t)}{v(k_t)} dk_t}{\int e_z \cdot v(k_t) \frac{dv(k_t)}{v(k_t)} dk_t}; \quad (12)$$

In Eqs. (11) and (12),  $\int$  denotes integration over the part of the Fermi surface with the relaxation time  $\tau_1$ . Equation (9) defines the plasma frequency  $\omega_p$  of the electron gas. The frequency  $\omega_H$  in Eq. (10) is proportional to the magnetic field  $H$ , however it does not coincide with the cyclotron frequency  $\omega_c$  except for a circular Fermi surface. Equations (6)-(8) represent the general form for  $\sigma_{xx}(\omega)$  and  $\sigma_{xy}(\omega)$  in the additive two-model and in

this general case correspond to a conventional two-band model. The equations contain six parameters: the prefactors  $a_1$  and  $a_2$ , the weights  $b_1$  and  $b_2$ , and the scattering times  $\tau_1$  and  $\tau_2$ . The dimensional parameters  $\omega_p$  and  $\omega_H$  determine the overall scale of  $\sigma_{xx}$  and  $\sigma_{xy}$ , whereas the time  $\tau_1$  sets the overall frequency scale. The remaining three dimensionless parameters  $a_1$ ,  $b_1$ , and  $\tau_2/\tau_1$  determine the shape of the frequency dependence. The frequency  $\omega$  appears in Eqs. (6) and (7) only through the effective times  $\tau_1(\omega)$  and  $\tau_2(\omega)$  defined in Eq. (8). At high frequencies  $\omega \gg \tau_{1,2}^{-1}$ , the two effective times coincide:  $\tau_1(\omega) = \tau_2(\omega) = \tau$ , and the model reduces to a simple Drude model. (The discussion of the high-frequency limit  $\omega \gg \tau_{1,2}^{-1}$  here and in the next paragraph is given only to illustrate the mathematical properties of the functions involved. It should not be applied literally to the high-frequency experiment, where the relaxation time  $\tau_1$  itself starts to depend on frequency:  $\tau_1 = \tau_1(\omega)$  [32,33].)

The additive two-model can describe the observed frequency dependence of the Hall coefficient  $R_H = \sigma_{xy}/\sigma_{xx}$ . As follows from Eqs. (6)-(8),  $\text{Re}R_H(\omega)$  starts at one value at  $\omega = 0$  and saturates to a different value at  $\omega = 1$ . While  $\text{Im}R_H = 0$  at  $\omega = 0$  and  $\omega = 1$ , it is in general nonzero at other frequencies. This is the qualitative behavior of the experimental data shown in the upper panel of Fig. 1. The ratio of the low- and high-frequency limits,

$$\frac{\text{Re}R_H(\omega = 0)}{\text{Re}R_H(\omega = 1)} = \frac{b_1 \tau_1^2 + b_2 \tau_2^2}{(a_1 \tau_1 + a_2 \tau_2)^2}; \quad (13)$$

can be fitted to the experimental value. On the other hand, in the additive two-model,  $\cot_H(\omega)$  cannot have an exactly linear dependence on  $\omega$ . However, it can have a dependence that is close to linear for special choices of the model parameters. This is in contrast to the multiplicative model (Eqs. (1) and (2)), which automatically produces  $\text{Re}\cot_H(\omega) = \text{const}$  and  $\text{Im}\cot_H(\omega) \propto \omega$ . This important distinction between the two models can be tested by measuring  $\cot_H(\omega)$  at different temperatures and verifying whether a linear frequency dependence exists at all temperatures.

We now discuss the analysis of the experimental data of Ref. [9] in terms of the additive two-model (6)-(8). Instead of fitting  $\cot_H$  and  $R_H$  deduced from the experimental data by Kramers-Kronig analysis, we fit the raw data shown in Fig. 2 by solid circles. The lower panel in this figure shows the transmission spectrum  $T(\omega)$  in zero magnetic field, and the upper panel gives the ratio of the transmittances  $T^+(\omega)$  and  $T^-(\omega)$  of circularly polarized light for two opposite orientations of the magnetic field:  $H = 9$  T and  $H = -9$  T. The transmission coefficient of a thin film of thickness  $D$  is related to conductivities (6) and (7) by the standard formula that takes into account multiple reflections in the substrate [9]:

$$T(\omega) = \frac{4nT_{\text{corr}}}{j\omega + n + Z_0 D (\sigma_{xx} - i\sigma_{xy})^2}; \quad (14)$$

where

$$T_{\text{corr}} = \frac{1 + R_s}{1 - R_s R (!)}; \quad (15)$$

$$R_s = \frac{n - 1}{n + 1}; \quad (16)$$

$$R (!) = \frac{1 - n + Z_0 D ( \epsilon_{xx} - i \epsilon_{xy} )^2}{1 + n + Z_0 D ( \epsilon_{xx} - i \epsilon_{xy} )}; \quad (17)$$

$Z_0 = 4\pi/c$  is the impedance of free space, and  $n$  is the substrate refraction index. The superscripts in Eqs. (14), (15), and (17) refer to the magnetic field parallel and antiparallel to the  $z$  axis.

Because the additive two-model has many adjustable parameters, we divide our fitting procedure into two stages and each stage into several steps. At the first stage we treat all six parameters of the two-model as independent variables. At this stage we examine how well the general additive two-model fits the experimental data. We consecutively optimize over the fitting parameters, leaving the optimization over  $a_1$  and  $b_1$  for the last step. At the second stage (Sec. III) we take into account that  $a_1$  and  $b_1$  are related to the electron dispersion law via Eqs. (11) and (12) and perform optimization for a model Fermi surface of  $\text{YBa}_2\text{Cu}_3\text{O}_7$ .

First we fit the transmittance spectrum in zero magnetic field,  $T (!)$ , which involves the parameters  $a_1$ ,  $\epsilon_1$ ,  $\epsilon_2$ , and  $\epsilon_p$ , but not  $b_1$  and  $\epsilon_H$ . For the fixed values of the parameters  $a_1 = 1$  and  $\epsilon_2 = \epsilon_1 > 1$ , we find the value of  $\epsilon_p(a_1; \epsilon_1)$  from  $T (! = 0)$  and the value of  $\epsilon_1(a_1; \epsilon_1)$  by minimizing the mean-square deviation between the theoretical and experimental data for  $T (!)$ :

$$\chi^2 = \frac{1}{N} \sum_{i=1}^N \frac{T^{(\text{exp})} (!_i) - T (!_i)^2}{T^{(\text{exp})} (!_i)}; \quad (18)$$

In Eq. (18) the sum is taken over the  $N$  experimental values of frequencies, the superscript (exp) denotes the experimental data, and  $T (!_i)$  refers to the theoretical values from the additive two-model. Then we scan the values of the parameters  $a_1$  and  $\epsilon_1$ , and retain for further consideration only those sets  $(a_1; \epsilon_1)$  where  $\chi^2 \leq 5\%$  and

6. The latter condition is imposed on the grounds that the scattering rate variation  $\epsilon_2 = \epsilon_1$  should not be too large, because a very strong variation of  $\epsilon_2$  would be hard to justify within the Fermi-liquid picture.

Next, for given values of  $a_1$  and  $\epsilon_1$ , we determine the parameters  $\epsilon_H$  and  $b_1$  in Eq. (7) by matching the two extremal points of the magnetic measurements:  $\text{Re} \cot \epsilon_H (! = 0) = 43$  and  $\text{Re} \epsilon_H (! = 0) = \text{Re} \epsilon_H (! = 200 \text{ cm}^{-1}) = 3$ . For a fixed value of  $a_1$ ,  $b_1 (!)$  is found to first increase with increasing  $\epsilon_1$  and then decrease. Thus,  $b_1$  does not exceed a certain maximal value that depends on  $a_1$ , and there exist two different values of  $\epsilon_1$  that generate the same value of  $b_1$  below the maximum. Again assuming that the scattering rate variation should not

be too large, we set  $\epsilon_1$  to the lower of these two values. With these restrictions, we can map the pair of variables  $(a_1; \epsilon_1)$  onto the pair  $(a_1; b_1)$  and use the latter as the pair of independent variables. To characterize the quality of a fit in magnetic field, we calculate the mean-square deviation between the experimental and theoretical data for  $r (!) = T^+ (!) = T (- !)$ :

$$\chi^2 = \frac{1}{N} \sum_{i=1}^N \frac{r^{(\text{exp})} (!_i) - r (!_i)^2}{r^{(\text{exp})} (!_i)}; \quad (19)$$

and present the contour plots of  $\chi^2_1(a_1; b_1)$  and  $\chi^2_2(a_1; b_1)$  in Fig. 3. The above listed constraints are satisfied in the  $(a_1; b_1)$  area below the dashed curve in Fig. 3. The contour lines of  $\chi^2_1(a_1; b_1)$  and  $\chi^2_2(a_1; b_1)$  intersect in a roughly orthogonal manner. The optimal fit of the experimental curves for  $T (!)$  and  $r (!)$  is achieved in the shaded area in Fig. 3, where both deviations between the theoretical and experimental data are minimal:  $\chi^2_1(a_1; b_1) < 2\%$  and  $\chi^2_2(a_1; b_1) < 0.3\%$ . The latter value is smaller than the experimental error bars approximately equal to 0.5%.

It was noticed in Ref. [9] that the zero-field transmittance  $T (!)$  can be well fitted with a simple Drude model. According to Fig. 3, the simple Drude model ( $a_1 = 1$ ) indeed provides a good fit for  $T (!)$  with  $\chi^2_1 = 3.5\%$ , but the additive two-model provides a better fit with  $\chi^2_1(a_1; b_1) < 2\%$ . While this is natural because the additive two-model has more fitting parameters, it does signify that small corrections to the simple Drude model are required to properly describe  $T (!)$ .

### III. MAPPING $\chi^2_1$ AND $\chi^2_2$ TO THE FERMI SURFACE OF $\text{YBa}_2\text{Cu}_3\text{O}_7$

In this section we will incorporate the band structure of  $\text{YBa}_2\text{Cu}_3\text{O}_7$  into our fitting procedure for the additive two-model. The band structure of  $\text{YBa}_2\text{Cu}_3\text{O}_7$  has been calculated by several groups [35-38]. The Fermi surface of this material is found to contain four sheets: the bonding and antibonding bands originating from the two  $\text{CuO}_2$  planes, the  $\text{CuO}$  chain band, and a small column-shaped (the so-called "stick") pocket originating from the  $\text{BaO}$  planes (see, for example, Fig. 2 in Ref. [37]). Photoemission measurements [39-42] agree qualitatively with the theoretical results, although the stick pocket was reported only in Ref. [39]. The chain band was observed in positron annihilation experiments [43], and the stick pocket has also been reported in the de Haas-van Alphen experiments [44]. Unfortunately, it is very difficult to extract the electron dispersion law in  $\text{YBa}_2\text{Cu}_3\text{O}_7$  from the photoemission measurements quantitatively [42]. Nevertheless, a best effort attempt was made by Schabel [45] for the  $\Gamma$ -S and X-S directions in the  $\text{YBa}_2\text{Cu}_3\text{O}_7$  Brillouin zone. The band-structure calculations [36,37] give the following values of the Fermi wave vector and velocity

along the  $\{S$  and  $X$   $\{S$  directions for the bonding  $\text{CuO}_2$  band at  $k_z = \pi/d$  [46]:  $k_F^{(\text{S})} = 0.9 \pi/a$ ,  $k_F^{(\text{X})} = 0.72 \pi/b$ ,  $v^{(\text{S})} = 0.6 \text{ eV}$ ,  $v^{(\text{X})} = 1.2 \text{ eV}$ , where  $a = 3.8 \text{ \AA}$  and  $b = 3.9 \text{ \AA}$  are the lattice constants of  $\text{YBa}_2\text{Cu}_3\text{O}_{7-x}$ . These values agree with the data of Schabel [45] within 10% for  $k_F$  and 25% for  $v_F$ .

This semiquantitative agreement with the photoemission experiment encourages us to use the band calculations of Refs. [36,37] in our analysis. We first calculate the contributions of each band to  $\sigma_{xx}$ ,  $\sigma_{yy}$ , and  $\sigma_{xy}$ , assuming that all bands have a single relaxation time  $\tau$  and using Eqs. (3) and (4) integrated over  $k_z$  from 0 to  $2\pi/d$ . The results are shown in Table I. The values of  $\tau$ ,  $\sigma_{xx}$ ,  $\sigma_{yy}$ , and  $R_H$  are in reasonable agreement with previous band-structure calculations [47]. As follows from Table I, the  $\text{CuO}_2$  bonding band gives maximal contribution to both the longitudinal and Hall conductivities. Thus, to simplify the analysis, we make the approximation of neglecting the contributions of the other bands and consider only the bonding band. The Fermi surface of the bonding band is shown in Fig. 4 for  $k_z = \pi/d$ . It contains the same geometrical features (large flat regions and sharp corners) that were discussed for the additive two-model in Refs. [4,5] (see Sec. I). The observed shape of the Fermi surface and the close values of the plasma frequencies,  $\omega_{px}^2 = 4.1 \times 10^{14} \text{ cm}^{-2}$  and  $\omega_{py}^2 = 4.5 \times 10^{14} \text{ cm}^{-2}$ , confirm that the bonding band has an approximate tetragonal symmetry. Strictly speaking, the conductivities should be calculated for a given value of  $k_z$  using the 2D formalism of Sec. II and then integrated over  $k_z$ . However, because the dispersion of the bonding band in the  $z$  direction is weak, we will simply use " $(k_x, k_y; k_z = \pi/d)$ " in the equations of Sec. II as the 2D electron dispersion law. We select the value  $k_z = \pi/d$ , since only for that value of  $k_z$  the  $\text{CuO}_2$  bonding band does not hybridize with the  $\text{CuO}$  chain band because of parity; thus, distortion of the plane band due to the chain band is minimal.

In mapping the additive two-model considered in Sec. II onto the bonding band of  $\text{YBa}_2\text{Cu}_3\text{O}_{7-x}$ , we must address two basic questions. First, is it possible to divide the Fermi surface of  $\text{YBa}_2\text{Cu}_3\text{O}_{7-x}$  in such a manner that the dimensionless weights  $a_1$  and  $b_1$ , calculated via Eqs. (11) and (12), have the values required by the additive two-model? An answer to this question depends only on the variation of the Fermi velocity  $v(k_t)$  over the Fermi surface, but not on the overall scale of  $v$ . Second, do the values of the dimensional parameters  $\omega_p$  and  $\omega_H$  for  $\text{YBa}_2\text{Cu}_3\text{O}_{7-x}$  agree with those in the additive two-model?

We assign the shorter relaxation time  $\tau_1$  to the large flat regions, making them "hot" with respect to relaxation, and the longer time  $\tau_2$  to the corners (bold lines in Fig. 4), making them "cold". This assignment, which is required to fit the ac and dc magnetotransport data from magnetic field along the  $c$  axis, is also consistent with the conclusions of the transport experiments with the

field in the ab plane [29]. To find an optimal decomposition of the Fermi surface into the hot and cold regions, we gradually increase the size of the cold regions symmetrically with respect to the  $\{S$  diagonal and calculate the weights  $a_1$  and  $b_1$  of the contribution of the hot regions to  $\sigma_{xx}$  and  $\sigma_{xy}$  from Eqs. (11) and (12). The weights  $a_1$  and  $b_1$  gradually decrease from 1 to 0, which generates the dotted curve in Fig. 3 labeled YBCO. The YBCO curve passes through the upper part of the shaded area in Fig. 3, where the deviation of the additive two-model from the experimental points is minimal. The solid square in Fig. 3 indicates the point of the best mapping of the  $\text{YBa}_2\text{Cu}_3\text{O}_{7-x}$  Fermi surface onto the additive two-model. The parameters of the additive two-model at this optimal point are given in Table II. The frequency dependences of  $T(\omega)$ ,  $r(\omega)$ ,  $R_H(\omega)$ , and  $\cot \theta_H(\omega)$ , generated in the additive two-model with this set of parameters, are shown by the solid lines in Figs. 2 and 1. These lines are in good agreement with the experimental points. Thus, the answer to the first question formulated earlier in this section is positive: The Fermi surface of  $\text{YBa}_2\text{Cu}_3\text{O}_{7-x}$  can be decomposed into the hot and cold regions in such a manner that the shape of the frequency dependences agrees well with the experiment.

Since the additive two-model with the parameters given in Table II fits the experimental data [9] very well, we will refer to the values in Table II as the experimental values. The value of the plasma frequency,  $\omega_p^{(\text{exp})} = 10^4 \text{ cm}^{-1}$ , in Table II is in reasonable agreement with the values  $\omega_{px} = 10^4 \text{ cm}^{-1}$  and  $\omega_{py} = 1.6 \times 10^4 \text{ cm}^{-1}$  found in previous measurements [48]. (Unlike [48], experiment [9] was performed on twinned samples of  $\text{YBa}_2\text{Cu}_3\text{O}_{7-x}$ , thus  $\omega_p^{(\text{exp})}$  is an average of  $\omega_{px}$  and  $\omega_{py}$ . The difference between  $\omega_{px}$  and  $\omega_{py}$  is mostly due to the  $\text{CuO}$  chains, which contribute predominantly to  $\omega_{py}$ , but not to  $\omega_{px}$ .) The values  $\omega_p^{(\text{exp})} = 10^4 \text{ cm}^{-1}$  and  $\omega_H^{(\text{exp})} = 1.7 \text{ cm}^{-1}$  from Table II differ considerably from the corresponding values found in the band structure calculations for the  $\text{CuO}_2$  bonding band:  $\omega_{px}^{(\text{bond})} = 2 \times 10^4 \text{ cm}^{-1}$  and  $\omega_H^{(\text{bond})} = 4 \text{ cm}^{-1}$  (see Table I). If  $a_1$ ,  $b_1$ ,  $\tau_1$ , and  $\tau_2$  from Table II are assigned to the  $\text{CuO}_2$  bonding band with  $\omega_p$  and  $\omega_H$  calculated in Table I, the discrepancies between the calculated and measured values are as follows:  $\sigma_{xx}^{(\text{bond})}(\omega) = \sigma_{xx}^{(\text{exp})}(\omega) = (\omega_p^{(\text{bond})}/\omega_p^{(\text{exp})})^2 = 4$  and  $R_H^{(\text{bond})}(\omega) = R_H^{(\text{exp})}(\omega) = (\omega_H^{(\text{bond})}/\omega_H^{(\text{exp})}) (\omega_p^{(\text{bond})}/\omega_p^{(\text{exp})})^2 = 0.6$ . (The ratios are frequency-independent, because the model matches the shape of the experimental frequency dependence.) The discrepancy between the calculated and experimental values of the plasma frequencies has been noticed and discussed in literature [47,48]. The simplest way to resolve this discrepancy is to assume that the Fermi velocity, proportional to  $\omega_p^2$  via Eq. (9), is uniformly reduced by a factor of 4 due to many-body renormalization effects coming from electron-phonon interaction or other correlation effects. Indeed, a factor of two to four renormalization

has been deduced from a memory function analysis of infrared data by Schlesinger et al. [33]. However, the uniform renormalization of the Fermi velocity cannot correct the discrepancy in the Hall coefficient, since  $R_H$  is not sensitive to the velocity scaling factor (see Eqs. (3) and (4)). Thus, the answer to the second question formulated earlier in this section is negative: The overall scales of the transport coefficients calculated for the band structure of  $\text{YBa}_2\text{Cu}_3\text{O}_7$  differ significantly from the measured values. Nevertheless, considering the crudeness of our model assumptions (discontinuous distribution of  $\tau$ , neglected contributions of other bands, and ignoring many-body renormalization effects), the qualitative and semiquantitative agreement of the fits indicates that the Fermi-liquid interpretation remains viable.

Every point  $k_t$  on a 2D Fermi surface has a certain Fermi velocity vector  $v(k_t) = (v_x(k_t); v_y(k_t))$ . As the point  $k_t$  moves along the Fermi surface, the 2D vector  $v(k_t)$  traces a certain curve in the 2D velocity space  $(v_x; v_y)$ . This curve is shown in Fig. 5 by the solid curve for the bonding band of  $\text{YBa}_2\text{Cu}_3\text{O}_7$ . The cold regions of the Fermi surface are indicated by the bold lines in Fig. 5. Correspondingly, the mean-free-path vector  $l(k_t) = (\ell_x; \ell_y)$  also traces a certain curve in the mean-free-path space  $(\ell_x; \ell_y)$  (the  $l$  curve). It was shown by Ong [34] that the Hall conductivity  $\sigma_{xy}$  of a 2D electron gas is proportional to the area enclosed by the  $l$  curve (see Eq. (4)). To illustrate the shape of the  $l$  curve, we multiply the Fermi velocity in the cold regions by the factor  $\alpha = \alpha_2 = \alpha_1 = 3.9$  and present the scaled curve by the dashed lines in Fig. 5. The  $l$  curve for the  $\text{YBa}_2\text{Cu}_3\text{O}_7$  bonding band is the same (up to the overall factor  $\alpha_1$ ) as the curve consisting of the dashed and thin lines in Fig. 5. This curve is qualitatively similar to the  $l$  curve found in Ref. [22] in the model of antiferromagnetic spin

fluctuations. On the other hand, our  $l$  curve differs from the  $l$  curve used in Refs. [4,5], where it was assumed the variation of  $l(k_t) = (\ell_x; \ell_y)$  is dominated by the variation of  $v(k_t)$ . Contrarily, we find that the variation of the scattering time  $\tau(k_t)$  outweighs the variation of the Fermi-surface velocity  $v(k_t)$ . Since the area of the sector enclosed by dashed lines in Fig. 5 is larger than the area enclosed by the thin curves, the Hall conductivity at zero frequency is dominated by the cold regions with the long relaxation time  $\tau_2$ . In the opposite limit of high frequency, the effective scattering times (8) become equal, and the contributions of the hot and the cold regions of the Fermi surface to the Hall conductivity  $\sigma_{xy}$  become comparable. In contrast, the longitudinal conductivity  $\sigma_{xx}$ , which is proportional to the mean-free-path average over the Fermi surface (3), is dominated by the hot regions of the Fermi surface in both high- and low-frequency limits.

Following Ref. [5], we assign linear and quadratic temperature dependences to the scattering rates of the additive two-model:

$$\tau_1^{-1} = T; \quad \tau_2^{-1} = T^2/W :$$

Using the values of  $\tau_1^{-1}$  and  $\tau_2^{-1}$  (see Table II) obtained by the fit of the ac Hall data to the additive two-model and taking into account that the measurements of Ref. [9] were taken at  $T = 95 \text{ K}$ , we find  $\alpha = 4.5$  and  $W = 82.5 \text{ K}$ . Using these and the other parameters listed in Table II, we calculate the temperature dependences  $\sigma_{xx}(T)$ ,  $R_H(T)$ , and  $\cot \theta_H(T)$  for the additive two-model and show them by the solid curves in Fig. 6. The top panel in Fig. 6 demonstrates a nearly linear temperature dependence of  $\sigma_{xx}(T)$ . The bottom panel shows the temperature dependence of  $\cot \theta_H$ . While not exactly quadratic, it does resemble the experimental data of Refs. [3,4]. With the assumed temperature dependences for the scattering times, we find that the two relaxation times become approximately equal at  $T = 371 \text{ K}$ :  $\tau_1(T = 371 \text{ K}) = \tau_2(T = 371 \text{ K})$ . Thus, we may expect Druide-like behavior for all frequency dependences at  $T = 371 \text{ K}$ , i.e.,  $\text{Re} R_H(\omega)$  to be approximately frequency-independent and  $\text{Im} R_H(\omega) \rightarrow 0$ .

In our discussion of the Hall effect, we have assumed the low-magnetic-field limit  $\mu_H \ll 1$ , where  $\mu_{xy}$  is given by Eq. (4) in terms of the distribution of the scattering time and the Fermi velocity over the Fermi surface. Using the parameters given in Table II, we find that for the moderate magnetic field of  $9 \text{ T}$  used in experiment [9]  $\mu_{H1} = 5.7 \cdot 10^3$  and  $\mu_{H2} = 2.2 \cdot 10^2$ , thus the low-field condition  $\mu_H \ll 1$  is indeed satisfied. On the other hand, in the strong-magnetic-field limit  $\mu_H \gg 1$ , the Hall coefficient is given by a different formula [1] in terms of the concentration of carriers (holes):

$$R_H = \frac{V}{2e c S}; \quad (20)$$

where  $S$  is the dimensionless fraction of the Brillouin zone enclosed by the Fermi surface, and  $V = abd$  is the unit-cell volume of the crystal [46]. For the bonding band of  $\text{YBa}_2\text{Cu}_3\text{O}_7$ , we find that  $S = 0.51$ , and the Hall coefficient in a strong magnetic field,  $R_H(\mu_H \gg 1) = 1.1 \cdot 10^9 \text{ m}^3/\text{C} = 0.3 R_H(\mu_H \ll 1)$ , is three times lower than in a weak magnetic field. The three-times reduction of the dc  $R_H$  from low to high magnetic fields is approximately the same as the reduction of  $R_H$  from low to high frequencies (see Fig. 1). Both effects have the common origin: The strong variation of  $\tau$  over the Fermi surface, essential for the Hall effect at low  $\omega$  and low  $H$ , becomes irrelevant for high  $\omega$  or high  $H$ . Recent experiment in overdoped  $\text{Tl}_2\text{Ba}_2\text{CuO}_{6+x}$  with  $T_c = 30 \text{ K}$  [49] found a decrease of  $R_H$  in a very strong field of  $60 \text{ T}$  where  $\mu_H = 0.9$ , in qualitative agreement with the theoretical picture outlined above.

We can also consider mapping of the additive two-model onto two distinct bands characterized by different relaxation times, for example the  $\text{CuO}_2$  bonding band and the  $\text{BaO}$  stick pocket. Assuming for simplicity that the bands have parabolic dispersion and using the parameters listed in Table II, we estimate the Fermi wave vectors, masses, and plasma frequencies of the corresponding bands:  $k_{F,1} = 0.84 \pi/a$  and  $k_{F,2} = 0.14 \pi/a$ ,  $m_1 = 6m$

and  $m_2 = 1.7m$ ,  $\omega_{p,1}^2 = 9 \cdot 10^7 \text{ cm}^{-1}$  and  $\omega_{p,2}^2 = 10^7 \text{ cm}^{-1}$ , where  $m$  is the free-electron mass. The values of the Fermi momenta roughly agree with the Fermi momenta of the  $\text{CuO}_2$  bonding band (see the beginning of this Section) and the BaO stick pocket ( $k_F^{(\text{stick})} = 0.11 \text{ \AA}^{-1}$  along the  $S(X)$  direction at  $k_z = \pi/d$ ) found in band-structure calculations [37], as well as the values  $0.12 \text{ \AA}^{-1}$  and  $0.17 \text{ \AA}^{-1}$  found in de Haas-van Alphen experiments [44] for  $k_F^{(\text{stick})}$ . The value of  $\omega_{p,1}$  differs significantly from the plasma frequency of the bonding band by about the same factor that we discussed earlier in this Section:  $\omega_{p,1}^2 = 0.2 (\omega_{p,x}^{(\text{bond})})^2$ , whereas  $\omega_{p,2}$  is comparable to the plasma frequency of the stick pocket,  $\omega_{p,2}^2 = 1.25 (\omega_{p,x}^{(\text{stick})})^2$ . However, de Haas-van Alphen experiments [44] give the value  $7m$  for the mass of the stick pocket, which strongly disagrees with the value required by the two-model. The contribution of the stick pocket to the Hall conductivity, 6% according to the band-structure calculations (see Table I), is too small compared with the value  $b_2 = 1/b_1 = 29\%$  required by the two-model (see Table II). In other words, to fit experiment [9], one needs a large and heavy Fermi surface, combined with a small and light one. On the contrary, band-structure calculations [37], as well as de Haas-van Alphen experiments [44], evince the large and light bonding Fermi surface, combined with the small and heavy stick Fermi surface. As a result, mapping of the additive two-model onto the  $\text{CuO}_2$  bonding band and the BaO stick pocket does not appear to be consistent with the ac and dc magnetotransport data.

#### IV. FITTING $\sigma_{xx}(\omega)$ AND $\sigma_{xy}(\omega)$ IN MULTIPLICATIVE TWO-MODELS

As mentioned in Sec. I, the experimental data of Ref. [9] can be well fitted by the multiplicative two-model defined by Eqs. (1) and (2). The charge-conjugation model [18] has the same multiplicative law for the Hall conductivity, but a different expression for the longitudinal conductivity:

$$\sigma_{xx}(\omega) = \frac{\omega_p^2}{2 [\tilde{\omega}_f(\omega) + \tilde{\omega}_s(\omega)]}; \quad (21)$$

$$\sigma_{xy}(\omega) = \frac{\omega_p^2 \omega_H}{4 \tilde{\omega}_f(\omega) \tilde{\omega}_s(\omega)}; \quad (22)$$

$$\tilde{\omega}_j(\omega) = \omega_j - i\Gamma_j; \quad j = f, s; \quad (23)$$

In this section, we fit the experimental frequency dependences  $T(\omega)$ ,  $r(\omega)$ ,  $R_H(\omega)$ , and  $\cot \theta_H(\omega)$  using both multiplicative two-models. Both models have four phenomenological parameters: the prefactors  $\omega_p$  and  $\omega_H$  and the relaxation rates  $\tau_f^{-1}$  and  $\tau_H^{-1}$  or  $\gamma_f$  and  $\gamma_s$ . In both formalisms, fitting the zero-field transmittance spectrum  $T(\omega)$  is equivalent to using a model with a single relaxation time, which we have already studied in Sec. II as

the special case  $a_1 = 1$ . That gives the following values of the parameters:  $\omega_p = 9.2 \cdot 10^3 \text{ cm}^{-1}$ ,  $\tau_{tr}^{-1} = (\gamma_f + \gamma_s)/2 = 185 \text{ cm}^{-1}$ , and  $\gamma_1 = 3.5\%$ . The zero-field transmittance spectrum  $T(\omega)$ , generated by these parameters, is shown by the dashed curve in the lower panel of Fig. 2. Then we find  $\omega_H$  by fitting  $\cot \theta_H(\omega = 0) = 43$  and find the ratio of the relaxation rates by minimizing the deviation  $\chi^2$  (see Eq. (19)). For the model (1)-(2), we find  $\omega_H^{-1} = 54 \text{ cm}^{-1}$ ,  $\omega_H^{-1} = 1.3 \text{ cm}^{-1}$ , and  $\gamma_2 = 0.22\%$ . For the charge-conjugation model (21)-(23), the values of the parameters are:  $\gamma_f = 322 \text{ cm}^{-1}$ ,  $\gamma_s = 49 \text{ cm}^{-1}$ ,  $\omega_H = 2 \text{ cm}^{-1}$ , and  $\gamma_2 = 0.29\%$ . The frequency dependences of  $R_H(\omega)$ ,  $\cot \theta_H(\omega)$ , and  $r(\omega)$  generated with these sets of parameters are shown in Figs. 1 and 2 by the dashed curves for the model (1)-(2) and by the dotted curves for the model (21)-(23). While both models are in reasonably good agreement with the experimental data, the fit to Anderson's model appears systematically better than the charge-conjugation model. Assigning the following temperature dependences to the scattering rates:  $\tau_{tr}^{-1}; \gamma_f/T$  and  $\omega_H^{-1}; \gamma_s/T^2$ , we obtain the temperature dependences  $\sigma_{xx}(T)$ ,  $R_H(T)$ , and  $\cot \theta_H(T)$  shown in Fig. 6 by the dashed lines for Anderson's model and by the dotted lines for the charge-conjugation model. The temperature dependences in all three models are relatively close to each other and agree qualitatively with the experiment.

#### V. CONCLUSIONS

In this paper we have examined various phenomenological interpretations of the ac Hall effect in the normal state of  $\text{YBa}_2\text{Cu}_3\text{O}_{7-x}$ . We have demonstrated that it is possible to fit the magnetotransport data obtained in Ref. [9] within a Fermi-liquid model, if different regions on the Fermi surface are characterized by two different relaxation times (the additive two-model). Mapping the additive two-model onto the  $\text{CuO}_2$  bonding band of  $\text{YBa}_2\text{Cu}_3\text{O}_7$  calculated in Refs. [36,37], we find that the large  $\pi$  regions of the Fermi surface have a short relaxation time (are "hot"), whereas the sharp corners have a long relaxation time (are "cold"). This distribution of the relaxation times over the Fermi surface of the  $\text{CuO}_2$  bonding band allows us to fit the shape of the experimental frequency dependences very well. On the other hand, there are considerable discrepancies between the band-structure calculations and the experiment in the overall magnitude of transport coefficients, which can be partially resolved by including many-body renormalization of the Fermi velocity.

We also find that the data of Ref. [9] can be well fitted by the two unconventional, multiplicative two-models: Anderson's 2D Luttinger-liquid model [11] generalized to finite frequencies by Kaplan et al. [9] and somewhat less well by the charge-conjugation-symmetry model by Coleman, Schofeld, and Tsvetlik [18]. We conclude that the

existing experimental data does not permit a definitive discrimination between these three models. Measurements of the frequency dependence of the ac Hall effect at different temperatures would be very useful. Since the relaxation rates have different temperature dependences, the frequency dependences of magnetotransport coefficients in the three models should change with temperature differently, so that discrimination between the different models may become possible.

#### ACKNOWLEDGMENTS

We are grateful to M. C. Schabel for sending us preprint [42] and unpublished data on the electron dispersion in  $\text{YBa}_2\text{Cu}_3\text{O}_7$  and to J. M. Harris and G. S. Boebinger for useful discussions. This work was supported by the David and Lucile Packard Foundation and by the NSF under Grants No. DMR-9417451 and DMR-9223217. The work at NRL was supported by the Office of Naval Research.

---

Electronic address anatoley@glueumd.edu.

<sup>y</sup> Electronic address yakovenk@glueumd.edu.

<sup>z</sup> Also at the Laboratory for Physical Sciences, College Park, Maryland 20740. Electronic address H.Drew@umailumd.edu.

- [1] A. A. Abrikosov, *Fundamentals of the Theory of Metals* (North-Holland, Amsterdam, 1988).
- [2] T. R. Chien, Z. Z. Wang, and N. P. Ong, *Phys. Rev. Lett.* **67**, 2088 (1991).
- [3] J. M. Harris, Y. F. Yan, and N. P. Ong, *Phys. Rev. B* **46**, 14293 (1992).
- [4] A. Carrington, A. P. Mackenzie, C. T. Lin, and J. R. Cooper, *Phys. Rev. Lett.* **69**, 2855 (1992); J. R. Cooper and J. W. Loram, *J. Phys. (Paris)* **16**, 2237 (1996).
- [5] C. Kendziora, D. Mandrus, L. Mahaly, and L. Forro, *Phys. Rev. B* **46**, 14297 (1992).
- [6] G. Xiao, P. Xiong, and M. Z. Cieplak, *Phys. Rev. B* **46**, 8687 (1992).
- [7] H. Takagi, B. Batlogg, H. L. Kao, J. Kwo, R. J. Cava, J. J. Krajewski, and W. F. Peck, Jr., *Phys. Rev. Lett.* **69**, 2975 (1992).
- [8] H. Y. Hwang, B. Batlogg, H. Takagi, H. L. Kao, J. Kwo, R. J. Cava, J. J. Krajewski, and W. F. Peck, Jr., *Phys. Rev. Lett.* **72**, 2636 (1994).
- [9] S. G. Kaplan, S. Wu, H.-T. S. Lihn, H. D. Drew, Q. Li, D. B. Fenner, J. M. Phillips, and S. Y. Hou, *Phys. Rev. Lett.* **76**, 696 (1996); H. D. Drew, S. Wu, and H.-T. S. Lihn, *J. Phys.: Condens. Matter* **8**, 10037 (1996).
- [10] Recently, the high-frequency Hall effect in the normal state of  $\text{YBa}_2\text{Cu}_3\text{O}_7$  was measured by B. Parks, S. Spielman, and J. Orenstein, *Phys. Rev. B* **56**, 115 (1997) using the time-domain spectroscopy. Wide distribution of experimental points in this work does not allow to make any quantitative conclusions about the frequency dependence.
- [11] P. W. Anderson, *Phys. Rev. Lett.* **67**, 2092 (1991).
- [12] An alternative generalization of Anderson's hypothesis to finite frequencies by D. B. Romero, *Phys. Rev. B* **46**, 8505 (1992) predicts a frequency-independent  $R_H$  (!), which does not agree with experiment [9].
- [13] J. M. Harris, Y. F. Yan, P. Matl, N. P. Ong, P. W. Anderson, T. Kinura, and K. Kitazawa, *Phys. Rev. Lett.* **75**, 1391 (1995).
- [14] Theory [12] effectively places  $\tau_r$  in front of the time derivative of the electron distribution function.
- [15] D. K. K. Lee and P. A. Lee, *J. Phys.: Condens. Matter* **9**, 10421 (1997).
- [16] E. Abrahams, *J. Phys. (Paris)* **16**, 2191 (1996).
- [17] G. Kotliar, A. Sengupta, and C. M. Varma, *Phys. Rev. B* **53**, 3573 (1996).
- [18] P. Coleman, A. J. Schofeld, and A. M. Tsvelik, *Phys. Rev. Lett.* **76**, 1324 (1996); *J. Phys.: Condens. Matter* **8**, 9985 (1996).
- [19] E. Lange, *Phys. Rev. B* **55**, 3907 (1997).
- [20] W. W. Schulz, P. B. Allen, and N. T. Privedi, *Phys. Rev. B* **45**, 10886 (1992).
- [21] A. Virostek and J. Ruvalds, *Phys. Rev. B* **42**, 4064 (1990); J. Ruvalds, *Supercond. Sci. Technol.* **9**, 905 (1996).
- [22] M. J. Lercher and J. M. Wheatley, *Phys. Rev. B* **52**, R7038 (1995).
- [23] R. Hlubina and T. M. Rice, *Phys. Rev. B* **51**, 9253 (1995).
- [24] B. P. Stojkovic and D. Pines, *Phys. Rev. Lett.* **76**, 811 (1996); *Phys. Rev. B* **55**, 8576 (1997); A. V. Chubukov, D. Pines, and B. P. Stojkovic, *J. Phys.: Condens. Matter* **8**, 10017 (1996).
- [25] T. Dahm, *Phys. Rev. B* **54**, 10150 (1996).
- [26] J. Altmann, W. Brenig, and A. P. Kampf, *cond-mat/9707267*.
- [27] N. P. Ong and P. W. Anderson, *Phys. Rev. Lett.* **78**, 977 (1997); B. P. Stojkovic and D. Pines, *ibid.* **78**, 978 (1997).
- [28] C. A. R. Sa de Melo, Z. Wang, and S. Doniach, *Phys. Rev. Lett.* **68**, 2078 (1992).
- [29] N. E. Hussey, J. R. Cooper, J. M. Wheatley, I. R. Fisher, A. Carrington, A. P. Mackenzie, C. T. Lin, and O. M. Ilat, *Phys. Rev. Lett.* **76**, 122 (1996).
- [30] A. T. Zheleznyak and V. M. Yakovenko, *Synth. Met.* **70**, 1005 (1995).
- [31] J. A. Clayhold, Z. H. Zhang, and A. J. Schofeld, *cond-mat/9708125*.
- [32] G. A. Thomas, J. Orenstein, D. H. Rapkine, M. Capizzi, A. M. Illis, R. N. Bhatt, L. F. Schneemeyer, and J. V. Waszczak, *Phys. Rev. Lett.* **61**, 1313 (1988).
- [33] Z. Schlesinger, R. T. Collins, F. Holtzberg, C. Feild, S. H. Blanton, U. Welp, G. W. Crabtree, Y. Fang, and J. Z. Liu, *Phys. Rev. Lett.* **65**, 801 (1990); Z. Schlesinger, R. T. Collins, F. Holtzberg, C. Feild, G. Koren, and A. Gupta, *Phys. Rev. B* **41**, 11237 (1990).
- [34] N. P. Ong, *Phys. Rev. B* **43**, 193 (1991).
- [35] W. E. Pickett, R. E. Cohen, and H. Krakauer, *Phys. Rev. B* **42**, 8764 (1990).
- [36] I. I. Mazin, A. I. Liechtenstein, C. O. Rodriguez,



- O. Jepsen, and O. K. Andersen, *Physica C* 209, 125 (1993).
- [37] O. K. Andersen, O. Jepsen, A. I. Liechtenstein, and I. I. Mazin, *Phys. Rev. B* 49, 4145 (1994).
- [38] O. K. Andersen, A. I. Liechtenstein, O. Jepsen, and P. Paulsen, *J. Phys. Chem. Solids* 56, 1573 (1995).
- [39] J. C. Cam puzano, G. Jennings, M. Faiz, L. Beaulaigue, B. W. Veal, J. Z. Liu, A. P. Paulikas, K. Vandervoort, H. Claus, R. S. List, A. J. Arko, and R. J. Bartlett, *Phys. Rev. Lett.* 64, 2308 (1990).
- [40] R. Liu, B. W. Veal, A. P. Paulikas, J. W. Downey, P. J. Kostic, S. Fleshler, U. Welp, C. G. Olson, X. Wu, A. J. Arko, and J. J. Joyce, *Phys. Rev. B* 46, 11056 (1992).
- [41] M. C. Schabel, C. H. Park, A. Matsuura, Z. X. Shen, D. A. Bonn, R. Liang, and W. N. Hardy, *Phys. Rev. B* 55, 2796 (1997).
- [42] M. C. Schabel, C. H. Park, A. Matsuura, Z. X. Shen, D. A. Bonn, R. Liang, and W. N. Hardy, unpublished.
- [43] M. Peter, A. A. Manuel, L. Homan, and W. Sadowski, *Europhys. Lett.* 18, 313 (1992); A. A. Manuel, A. Shukla, L. Homan, T. Jarlborg, B. Barbiellini, S. Massidda, W. Sadowski, E. Walker, A. Erb, and M. Peter, *J. Phys. Chem. Solids* 56, 1951 (1995).
- [44] C. M. Fowler, B. L. Freeman, W. L. Hults, J. C. King, F. M. Mueller, and J. L. Smith, *Phys. Rev. Lett.* 68, 534 (1992); E. G. Haanappel, W. Joss, P. Wyder, S. Akenazy, F. M. Mueller, K. Trubench, H. J. Mattausch, A. Simon, and M. Osofsky, *J. Phys. Chem. Solids* 54, 1261 (1993); E. G. Haanappel, W. Joss, I. D. Vagner, P. Wyder, K. Trubench, H. J. Mattausch, A. Simon, F. M. Mueller, and S. Akenazy, *Physica C* 209, 39 (1993).
- [45] M. C. Schabel, Ph.D. thesis, Stanford University, 1997.
- [46] In Sec. III we use the letter  $d$  to denote the lattice spacing of  $\text{YBa}_2\text{Cu}_3\text{O}_7$  in the  $c$  direction, not the distance between  $\text{CuO}_2$  layers. This spacing is usually denoted by the letter  $c$ , but we reserve that letter for the speed of light.
- [47] P. B. Allen, W. E. Pickett, and H. Krakauer, *Phys. Rev. B* 37, 7482 (1988).
- [48] D. N. Basov, R. Liang, D. A. Bonn, W. N. Hardy, B. Dabrowski, M. Quijada, D. B. Tanner, J. P. Rice, D. M. Ginsberg, and T. Timusk, *Phys. Rev. Lett.* 74, 598 (1995).
- [49] A. W. Tyler, Y. Ando, F. F. Balakirev, A. Passner, G. S. Boebinger, A. J. Schoeld, A. P. Mackenzie, and O. Laborde, cond-mat/9710032.

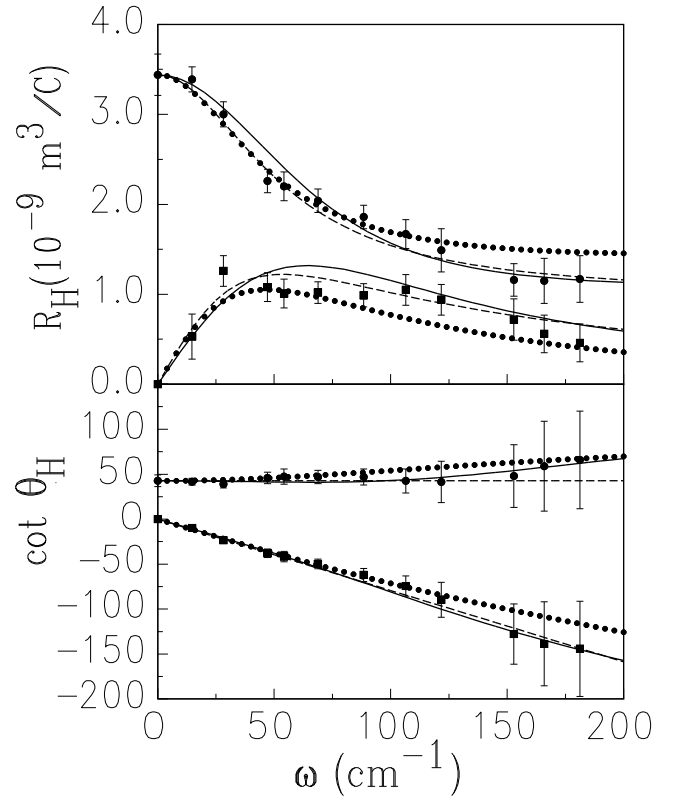


FIG. 1. Frequency dependence of real and imaginary parts of the inverse Hall angle  $\cot \theta_H$  (lower panel) and the Hall coefficient  $R_H$  (upper panel). Experimental values from Ref. [9] are represented by the solid circles (real parts) and the solid squares (imaginary parts). The solid, dashed, and dotted curves show the frequency dependences generated by the additive two-band model (Eqs. (6)-(8)), by the multiplicative two-band model (Eqs. (1) and (2)), and by the charge-conjugation model (Eqs. (21)-(23)), respectively.

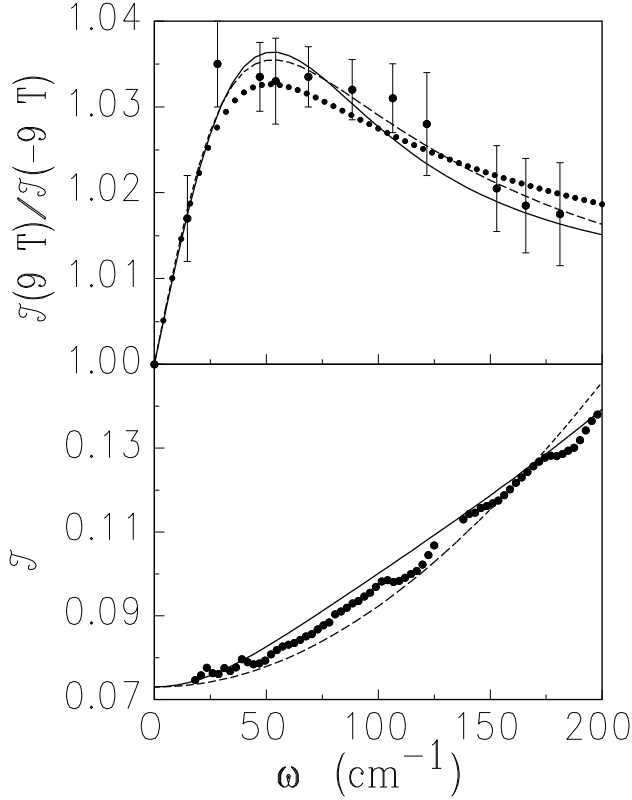


FIG. 2. Far-infrared transmission spectra of a  $\text{YBa}_2\text{Cu}_3\text{O}_7$  thin film. The lower panel gives the frequency dependence of the transmission  $T(\%)$  in zero magnetic field. The upper panel shows the ratio of the transmissions at  $H = 9$  and  $H = -9$  T. The solid circles represent the experimental values from Ref. [9]. The solid curves show the frequency dependences generated by the additive two- $\omega$  model (6)–(8). The dashed and the dotted curves in the upper panel represent the multiplicative two- $\omega$  model (Eqs. (1) and (2)) and the charge-conjugation model (Eqs. (21)–(23)), respectively. The dashed curve in the lower panel is obtained in the single-relaxation-time Drude model.

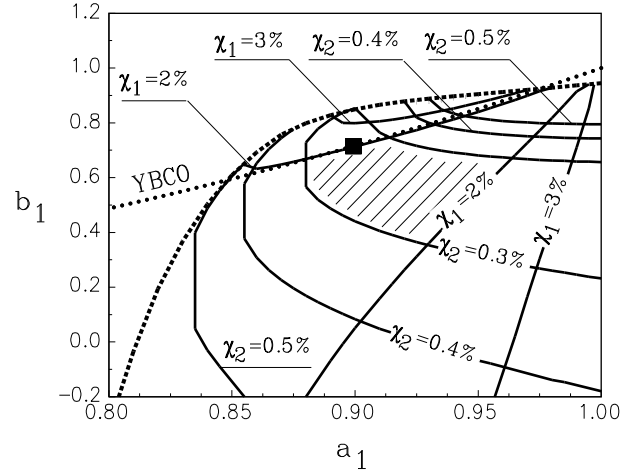


FIG. 3. Contour plots of  $\chi_1(a_1; b_1)$  (Eq. (18)) and  $\chi_2(a_1; b_1)$  (Eq. (19)) shown by the solid lines. Both  $\chi_1(a_1; b_1)$  and  $\chi_2(a_1; b_1)$  are minimal in the shaded area:  $\chi_1 < 2\%$  and  $\chi_2 < 0.3\%$ . Various constraints listed in Sec. II are satisfied below the dashed line. The dotted line, labeled YBCO, illustrates the relation between  $a_1$  and  $b_1$  for the  $\text{CuO}_2$  bonding band of  $\text{YBa}_2\text{Cu}_3\text{O}_7$ . The solid square denotes the best mapping of the additive two- $\omega$  model onto the  $\text{CuO}_2$  bonding band of  $\text{YBa}_2\text{Cu}_3\text{O}_7$ .

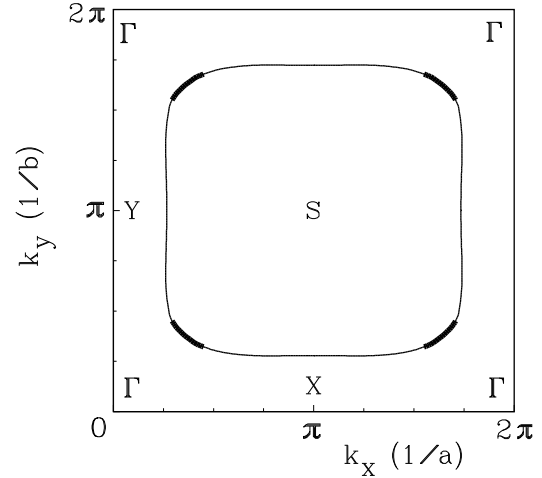


FIG. 4. Fermi surface of the  $\text{CuO}_2$  bonding band of  $\text{YBa}_2\text{Cu}_3\text{O}_7$  for  $k_z = \pm d$  according to the band-structure calculations of Ref. [37]. The regions denoted by the thin lines have the short scattering time  $\tau_1$ , whereas the bold regions have the long scattering time  $\tau_2$ .

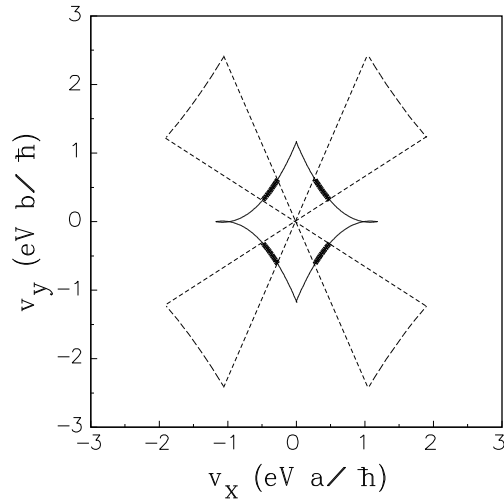


FIG. 5. Solid lines: distribution of the Fermi velocity vector  $(v_x; v_y)$  for the  $\text{CuO}_2$  bonding band of  $\text{YBa}_2\text{Cu}_3\text{O}_7$  according to the band-structure calculations of Ref. [37] for  $k_z = \pi/2$ . Bold lines: regions with the long scattering time  $\tau_2$ . Dashed lines: the Fermi velocity scaled by the factor of  $\tau_2/\tau_1 = 3.9$ . The area enclosed by the dashed and thin lines determines the zero-frequency Hall conductivity via Ong's formula [34].

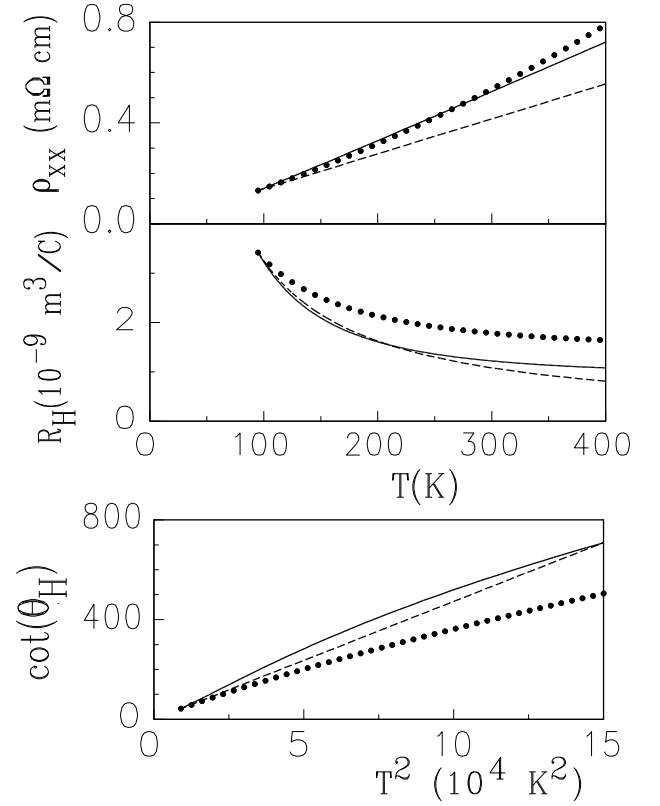


FIG. 6. Temperature dependences of resistivity  $\rho_{xx}$  (top panel), the Hall coefficient  $R_H$  (middle panel), and the inverse Hall angle  $\cot \theta_H$  at  $H = 9 \text{ T}$  (bottom panel), generated in the additive and multiplicative two-models by assigning  $\tau_1^{-1}$ ,  $\tau_{tr}^{-1}$ ,  $\tau_f^{-1}/T$  and  $\tau_2^{-1}$ ,  $\tau_H^{-1}$ ,  $\tau_s^{-1}/T^2$ . The solid, dashed, and dotted curves correspond to the additive, multiplicative, and charge-conjugation models, respectively.

TABLE I. Contributions of different YBa<sub>2</sub>Cu<sub>3</sub>O<sub>7</sub> bands to the longitudinal and Hall conductivities in a single-relaxation-time model. As it is conventional in optics, the frequencies are given in cm<sup>-1</sup>. The plasma frequencies  $\omega_{px}$  and  $\omega_{py}$  are taken from Ref. [36].

	Total	Bonding CuO <sub>2</sub> band	Antibonding CuO <sub>2</sub> band	Chains CuO band	Stick BaO pocket
$4 \quad \chi_{xx} = \omega_{px}^2$	$7 \cdot 10^8 \text{ cm}^{-2}$	59%	36%	4%	1%
$4 \quad \chi_{yy} = \omega_{py}^2$	$12 \cdot 10^8 \text{ cm}^{-2}$	37%	32%	30%	1%
$4 \quad \chi_{xy} = 2 \text{ at } H = 9 \text{ T}$	$2 \cdot 10^9 \text{ cm}^{-3}$	82%	40%	28%	6%
$R_H = \chi_{xy} / (\chi_{xx} - \chi_{yy})$	$0.16 \cdot 10^{-9} \text{ m}^3/\text{C}$				

TABLE II. Parameters of the additive two- model for the best mapping onto the YBa<sub>2</sub>Cu<sub>3</sub>O<sub>7</sub> Fermi surface.

$a_1$	$b_1$	$\omega_2 = \omega_1$	$\omega_1^1$	$\omega_2^1$	$\omega_p$	$\omega_H \text{ at } H = 9 \text{ T}$	$\omega_1$	$\omega_2$
0.9	0.71	3.9	$297 \text{ cm}^{-1}$	$76 \text{ cm}^{-1}$	$10^4 \text{ cm}^{-1}$	$1.7 \text{ cm}^{-1}$	2%	0.3%